Arab J Geosci (2016) 9: 665
DOI 10.1007/s12517-016-2684-3

ORIGINAL PAPER

Rhönite in undersaturated alkaline gabbroic rocks, Central Alborz, North Iran: petrography and mineral chemistry

Roghieh Doroozi[1] · **Carmela Vaccaro**[2] · **Fariborz Masoudi**[1]

Received: 3 February 2016 / Accepted: 19 September 2016 / Published online: 8 October 2016

Abstract The Kamarbon alkaline gabbroic intrusion crops out in Central Alborz, north Iran, along the northern margin of the Alpine-Himalayan belt. The gabbroic intrusion includes theralites at margins which replace with teschenites toward the center. In teschenitic rocks, the main minerals are diopside, clinopyroxene, and rhönite. In this research, the occurrence of rhönite is reported in Kamarbon teschenitic gabbros, and also its mineralogical properties, paragenesis, and source magma are investigated. Based on whole rock and microprobe analysis data, we try to clarify the formation of Kamarbon gabbro and the crystallization condition of rhönite. In teschenitic gabbros, rhönite reveals the composition $(Na, Ca)_{1.97}(Ti, {}^{VI}Al, Fe^{+3}, Fe^{+2}, Mn, Mg)_{5.99}(Si, {}^{IV}Al)_{6.02}O_{20}$. On the basis of petrographical observations and mineral chemistry, we suggest that the teschenites were formed in distinctive lower pressures and temperatures than theralites, below 1.9 kbar and 1075 °C. Rhönite was crystallized (at the mentioned P-T condition) as a primary phase, in the late stage of crystallization at shallow depth corresponding with 6–10 km, in teschenites. Important factors of the rhönite crystallization in undersaturated magmas can be regardarded as Al and Ti enrichment and Si depletion; the same enrichment and depletion are also observed in the associated clinopyroxenes.

Keywords Rhönite · Theralite · Teschenite · Crystallization · Central Alborz

✉ Roghieh Doroozi
r.doroozi220@gmail.com

[1] Faculty of Earth Science, Shahid Beheshti University, Velenjak, Tehran, Iran

[2] Istituto di Mineralogia, Universita di Ferrara, C.so E. 10 d'Este 32, 44100 Ferrara, Italy

Introduction

Alkaline magmas reveal various compositions and include different minerals. Investigating the minerals of alkaline magmas could lead to gain a better understanding of their chemical compositions and genesis. The presence of feldespatoid minerals is a frequent characteristic of undersaturated alkaline magmas (Dostal and Owen 1998). Rhönite is a mineral that belongs to the sapphirine supergroup, is observed in igneous undersaturated rocks (Deer et al. 1978), and is an inosilicate mineral with the crystallization in triclinic system (Walenta 1969). Rhönite reveals the general formula of $X_2Y_6Z_6O_{20}$ in which X = Na, K, and Ca; Y = Ti, ${}^{VI}Al$ ${}^{VI}Fe^{+3}$; Fe^{+2}, Mn, and Mg; and Z = Si, ${}^{IV}Al$, and ${}^{IV}Fe^{+3}$ (Kelsey and McKie 1964; Mineral Publishing Data 2001; Grew et al. 2008). Diopside, titanaugite, kaersutite, forsterite, spinel, perovskite, nepheline, leucite, analcime, and titanomagnetite are considered its associated minerals (Walenta 1969). Rhönite is the only sapphirine group mineral which take either $Mg/(Mg + Fe^{+2}) < 0.5$ or $Mg/(Mg + Fe^{+2}) > 0.5$. Most of rhönites reveal $Mg/(Mg + Fe^{+2}) > 0.5$, which can be termed rhönite with the end-member composition $Ca_2(Mg_4Fe^{+3}Ti)O_2[Si_3Al_3O_{18}]$ (Grew et al. 2008).

This mineral is reported mostly in volcanic rocks like basanites and alkaline basalts (Lacroix 1909; Babkine et al. 1964; Cameron et al. 1970; Grünhagen and Seck 1972; Kyle and Price 1975; Brooks et al. 1979; Boivin 1980; Havette et al. 1982; Olsson 1983; Bonaccorsi et al. 1990; Sharygin 2002; Grapes et al. 2003; Jannot et al. 2005; Kogarko et al. 2005) and rarely in plutonic rocks like alkaline gabbros (Johnston and Stout 1985; Kuehner and Irving 2007). We report the occurrence of rhönite in Kamarbon alkaline plutonic intrusion in Central Alborz, north Iran and investigate this mineral characteristics, paragenesis, and parental magma, based on both rhönite

microprobe and whole rock analysis. The genesis and geochemical properties of the alkaline magmatisim in Central Alborz could be cleared by the study on rhönites. These data also provide an opportunity to identify the possible occurred substitutions though rhönite composition. Results of this study may help to have a better understanding of the alkaline magmatism that produced the alkaline plutonic intrusions in Alpine-Himalayan orogenic belt in Central Alborz.

Geologic background

Central Alborz was a part of the Gondwana plate in Early Paleozoic. It separated from Gondwana during Ordovician to Silurian and then collided with Eurasian plate in Triassic, causing the Paleotethys Ocean closure to the north and the formation of the Neotethys Ocean to the south (Stocklin 1974; Berberian and King 1981; Stampfli et al. 1991). After the Triassic collisional event, along both sides of the Paleotethys Ocean, intracontinental compressions were initiated and accompanied by deposition of coal-bearing Jurassic shales (Berberian 1983).

In Central Alborz, Mesozoic era began with the deposition of detrital carbonate sediments which is continued with deposition of shales in Upper Triassic. In the studied area, extensional phases were started in Upper Triassic associated with alkaline igneous activity. This alkaline magmatic phase can be assumed as an evidence for intracontinental tectonic setting related to a rift system in Central Alborz during Late Triassic (Furon 1941; Steiger 1966; Taraz 1974; Nabavi and Seyed emami 1977; Kristan-Tollmann et al. 1979; Berberian and king 1981; Berberian 1983; Annels et al. 1985; Völlmer 1987; Fauvelet and Eftekhar Nezhad 1992; Sabzehei 1993; Seyed emami 2003; Brunet et al. 2003; Shahidi 2005, 2008; Nazari and Shahidi 2011).

Extensional movements started at the same time with Rhaetic rift volcanism and deposition of coal-bearing shales, in Mesozoic era, in Central Alborz (Berberian 1983; Nazari et al. 2004). The extensional phases developed some regional rifts which caused volcanism and plutonism activities in Central Alborz (Berberian 1983).

Soffel and Förster (1984) believe that the extensional movements lead to separation of the Central Iranian plate from Eurasia plate, during Jurassic. Lithospheric ruptures, tensions, and extensions with upwelling and decompressional melting of an asthenospheric mantle caused the development of the rift system in Alborz zone from Middle Jurassic to Lower Cretaceous (Haghnazar 2009; Ansari et al. 2011).

In the literature regarding Kamarbon alkaline intrusion in Central Alborz, there is no corresponding radiometric ages available but a rather poorly constrained Late Triassic to Upper Jurassic age is proposed (Saeedi 1993).

Regional geology and field occurrences

Alborz Mountains are a geological structural zone in north of Iran considered part of the northern margin of the Alpine-Himalayan orogenic belt (Fig. 1). Alborz block is connected to Caucasus Mountains in the northwest and is bounded by Hindu Kush Mountains in the east (Zanchi et al. 2006), which was part of the Gondwana plate in early Paleozoic. During Ordovician to Silurian, Alborz separated from Gondwana and finally collided with the Eurasia plate in Triassic (Alavi 1991; Stampfli 1996, 2000). So, the Alborz block can be considered an active mountain belt which is the consequence of Gondwana and Eurasia plate collision in Triassic (Stocklin 1974; Berberian and King 1981; Sengör et al. 1988; Sengör 1990; Stampfli et al. 1991; Sengör and Natalin 1996; Guest et al. 2006).

The study area is located in the northern part of Alborz structural zone that is called Central Alborz (Fig. 1). Central Alborz is composed of Paleozoic to Quaternary sedimentary rocks, wide range of Paleozoic to Quaternary volcanic rocks and some outcrops of metamorphic rocks in the northern border line. Intrusions are also common in this area, with the prevailing age of Paleocene and Oligocene. A sequence of Precambrian to Cretaceous sedimentary rocks with some unconformities and hiatuses are reported in Central Alborz.

The oldest rocks in the study area are Precambrian schists and slates of Kahar Formation (Alavi 1996). Permian sediments occur in Central Alborz zone accompanied by some volcanic, subvolcanic, and pyroclastic basaltic and andesitic rocks (Vahdati Daneshmand 2004). Massive Triassic dolomites of Elika Formation with a minor basic volcanic activity are the deposits of lower Mesozoic era. Jurassic shales of Shemshak Formation are widespread and overlap Precambrian, Upper Triassic, and Middle Triassic deposits with angular unconformity (Cartier 1971).

In the eastern part of the study area, the emplacement of several small gabbroic intrusions in the Shemshak Formation is reported (Saeedi 1993). The main outcrop of Kamarbon gabbro (approximately 4.5*3 km) occurs in the Shemshak Formation in the south of Kamarbon village in the longitudes 51° 21′ to 51° 25′ and latitudes 36° 14′ to 36° 16′ (Fig. 1).

The intrusion reveals flat form at margins, mostly covered by the Jurassic Shemshak Formation. No clear contact metamorphic aureole observed. The margins reveal fine granular gabbros with an average grain size of 1 mm and thickness of approximately 1.5 km but toward the center the average grain size rises up to 3 cm (Fig. 2).

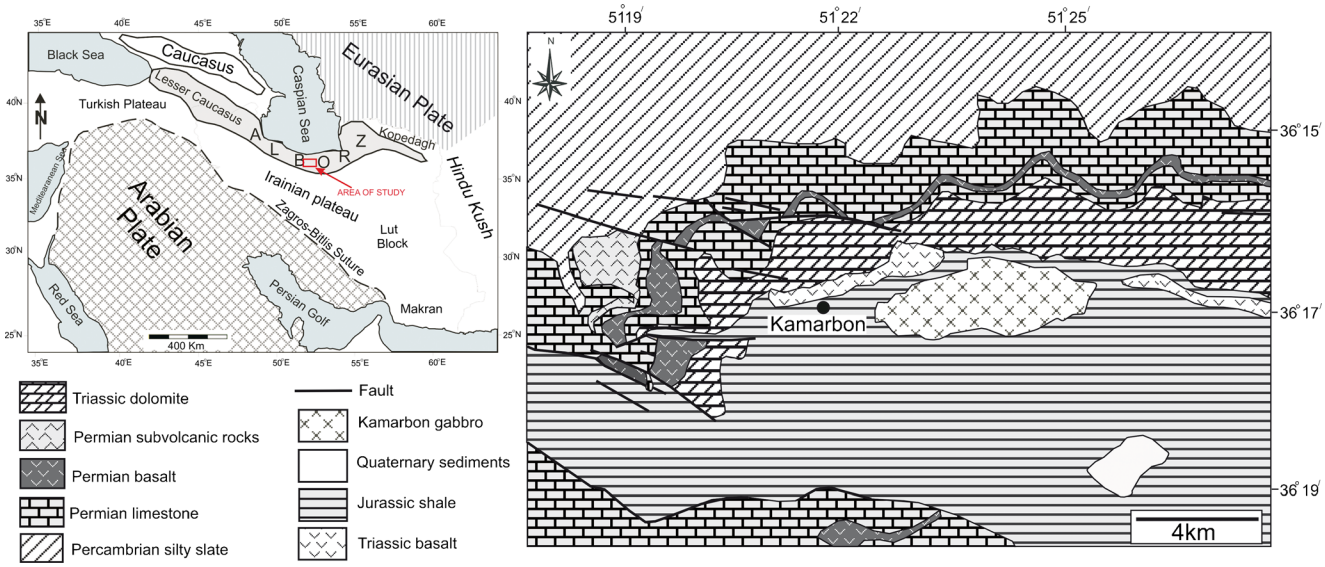

Fig. 1 Geological map of the study area. Modified from the geological map of 1/100,000 Marzanabad, Iran

Analytical methods

Fresh rock chips samples were collected and powdered in the agate mill. The X-ray fluorescence (XRF) analysis for major elements was done on powder pellets of rock samples, using a wavelength-dispersive automated Philips PW 1400 spectrometer at the Department of Earth Sciences (Ferrara University), using the method by Franzini et al. (1975) and Leoni and Saitta (1976). Rare Earth Elements (REE), Y, Zr, Hf, Nb, Ta, Th, and U were analyzed by inductively coupled mass spectrometry (ICP-MS) in the same department, using a VG Plasma Quad2 plus. Accuracy and precision, based on the replicated analyses of samples and standards, are estimated as better than 10 % for all elements well above the detection limit.

Mineral compositions were measured at the Department of Mineralogy (Padua University) with a Cameca-Camebax electron microprobe (fitted with three spectrometers) at

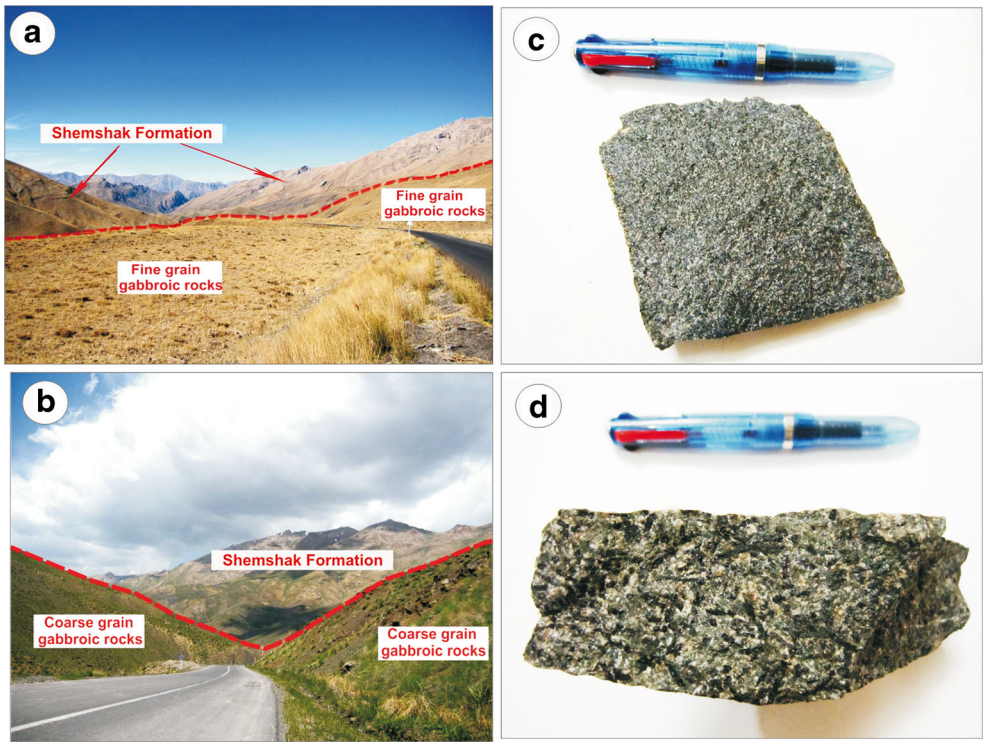

Fig. 2 Field and hand specimen pictures of **a, c** fine-grained gabbros and **b, d** coarse-grained gabbros

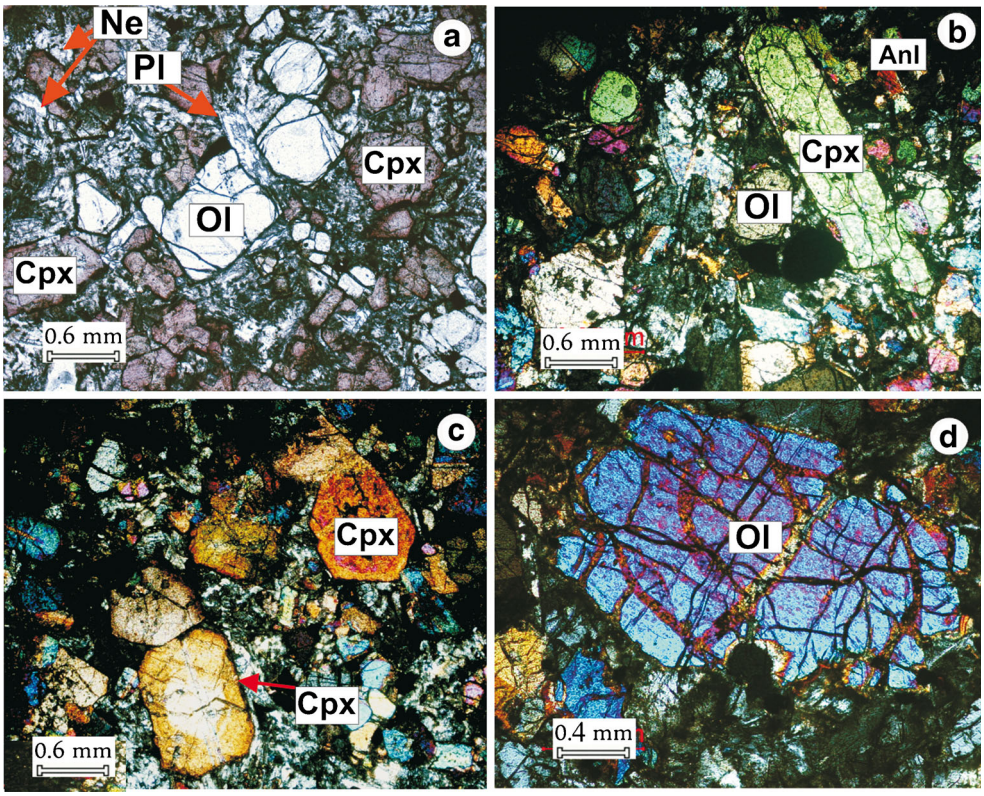

Fig. 3 Olivine (*Ol*), clinopyroxene (*Cpx*), nepheline (*Nph*) and plagioclase (*Pl*) in Kamarbon theralite gabbros. **a** Plane-polarized light image. **b**–**d** Cross-polarized transmitted light images

accelerating voltage of 15 kV, and specimen current of 15 nA, using natural silicates and oxides as standards. The beam was enlarged to a diameter of 5 μm and the counting times were set to 10 s for both peak and background and the data correction was performed using PAP methods (Pouchou and Pichoir 1984).

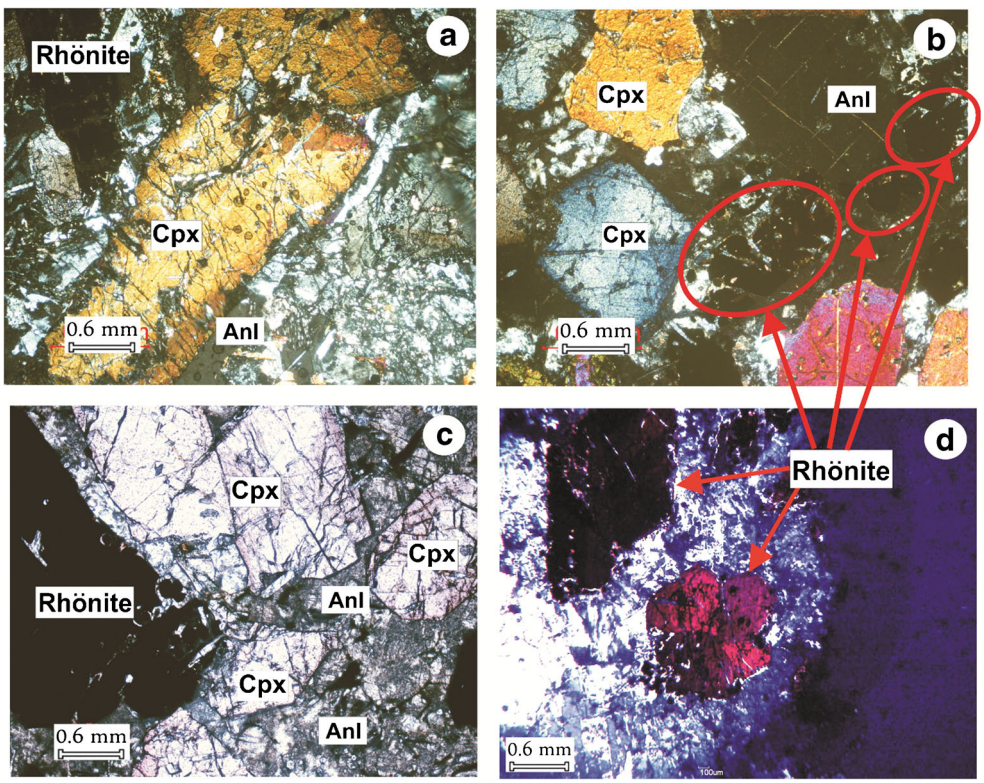

Fig. 4 pyroxene (*Cpx*), plagioclase (*Pl*), analcime (*Anl*), and rhönite in Kamarbon teschenite gabbros. **c** Plane-polarized light image. **a**, **b**, **d** Cross-polarized transmitted light images

Table 1 Microprobe analysis of rhönites in Kamarbon teschenite gabbro

Sample	RD172	RD172	RD172	RD172	RD182	RD182	RD182	RD168	RD168	RD168	RD168
Rock type	Tes	Tes	Tes	Tes	Tes	Tes	Tes	Tes	Tes	Tes	Tes
SiO_2	24.62	24.08	23.4	24.4	23.67	24.11	24	24.31	23.6	23.81	24.19
TiO_2	10.69	10.73	10.67	10.59	10.38	10.51	10.89	10.38	10.58	10.5	10.45
Al_2O_3	17.32	17.52	17.34	17.29	17.76	17.91	17.45	17.67	18.03	17.78	16.08
Cr_2O_3	bdl	bdl	0.01	0.01	0.01	0.03	0.02	0.02	bdl	0	0.39
FeO	22.37	22.66	27.26	22.62	21.78	22.24	22.57	22.63	22.68	22.28	22.25
MnO	0.21	0.19	0.34	0.22	0.22	0.17	0.15	0.19	0.24	0.23	0.16
MgO	11.68	12.04	8.07	11.76	12.71	12.26	11.44	12.02	11.94	12.1	10.34
CaO	11.98	12.19	11.77	12.04	12.1	12.25	11.98	12.21	12.2	12.07	11.31
Na_2O	0.93	0.89	0.91	0.95	0.87	0.87	0.89	0.85	0.86	0.81	1.01
K_2O	bdl	0.01	bdl	bdl	0.03	0.02	bdl	bdl	0.01	0.01	bdl
Total	99.8	100.31	99.75	99.88	99.52	100.36	99.39	100.28	100.14	99.58	96.19
Si	3.31	3.22	3.23	3.28	3.17	3.21	3.25	3.25	3.16	3.2	3.4
Ti	1.08	1.08	1.11	1.07	1.05	1.05	1.11	1.04	1.07	1.06	1.11
Al	2.78	2.76	2.82	2.74	2.8	2.81	2.78	2.78	2.85	2.82	2.66
Cr^{3+}	0.00	0.00	0.00	0.00	0.00	0.00	0.00	0.00	0.00	0.00	0.04
Fe^{3+}	0.7	0.86	0.74	0.8	0.99	0.87	0.73	0.84	0.92	0.86	0.55
Fe^{2+}	1.82	1.66	2.41	1.74	1.45	1.61	1.82	1.68	1.61	1.65	2.06
Mn	0.02	0.02	0.04	0.02	0.02	0.02	0.01	0.02	0.03	0.03	0.02
Mg	2.34	2.4	1.66	2.36	2.54	2.44	2.31	2.39	2.38	2.43	2.17
Ca	1.72	1.75	1.74	1.73	1.74	1.75	1.73	1.75	1.75	1.74	1.7
Na	0.24	0.23	0.24	0.25	0.23	0.22	0.22	0.22	0.22	0.21	0.28
K	0.00	0.00	0.00	0.00	0.00	0.00	0.00	0.00	0.00	0.00	0.00
Total	14.02	13.98	13.99	13.99	13.99	13.98	13.97	13.97	13.98	14	13.99
No. Mg	0.56	0.59	0.41	0.58	0.64	0.6	0.56	0.59	0.6	0.6	0.51

Caculation is based on 20 oxygens. (Tes is symbole of teschenitic gabbros)

Field geology and petrography

At margins, the fine-grained gabbros include olivine, clinopyroxene, plagioclase, and nepheline, plus minor accessory apatite and analcime (Fig. 3). Clinopyroxene which is the most abundant mineral in fine-grained gabbros, represents zoning structure (Fig. 3c), whereas some olivines show mesh texture (Fig. 3d). Olivine is the second most abundant mineral which usually is less than 1 mm grain size; although some of them may be up to 2 cm. Interstitial euhedral and subhedral nephelines are crystallized between olivines and pyroxenes.

The coarse-grained gabbros at the center contain clinopyroxene, rhönite, plagioclase, and analcime plus accessory apatite, nepheline, olivine, and alkali feldspar (Fig. 4), whereas some clinopyroxene rims show alteration to opaque minerals. Rhönite is the second abundant mineral which is similar to opaque minerals and observes in silica-undersaturated alkaline igneous rocks. It is almost opaque and exhibits a red-brown color at thinner crystal edges (Fig. 4d). Pleochroism is dark reddish brown or black. The size of euhedral rhönites can reach up to 3 cm in the central part of intrusion. Plagioclases show some alterations of sericite, albite, and calcite. Between pyroxenes and rhönites, there are crystallized anhedral analcimes (Fig. 4b, c).

The amount of mafic minerals such as olivine and clinopyroxene decreases toward the center of the intrusion while the amount of felsic minerals such as nephelines, analcimes, and more sodic plagioclases increases. The main mineral components of gabbroic rocks are rather fresh except plagioclases which represent partly sericitization and albitization.

Based on mineralogical studies, the gabbroic intrusion includes fine-grained theralite gabbro at the margin which replaces with coarse-grained teschenite gabbro at the center.

Mineral geochemistry

Rhönite

Microprobe analyses of rhönites are represented in Table 1. The structural formula recalculation is done on the basis of 14 cations

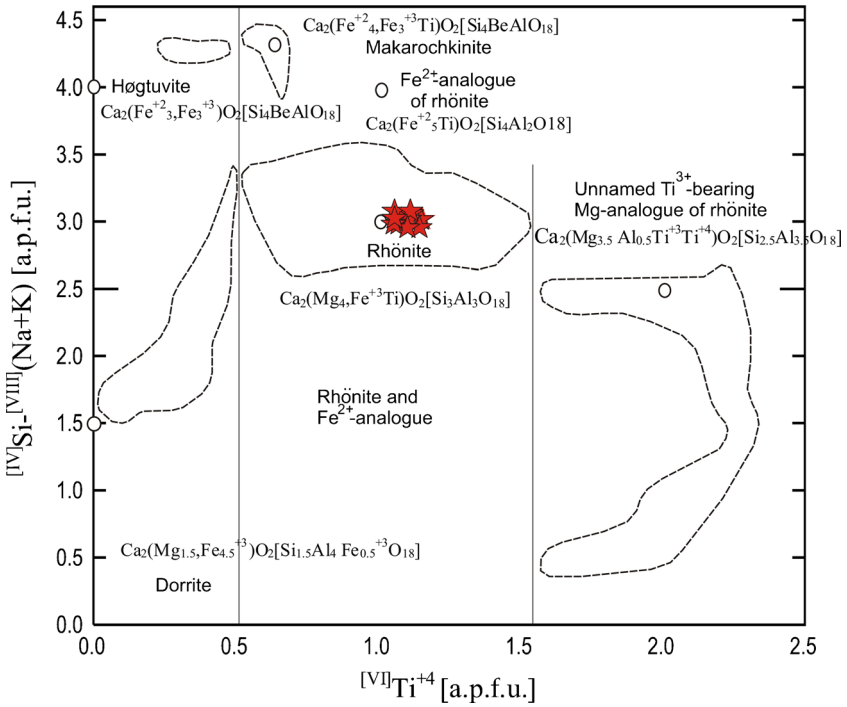

Fig. 5 Plot of rhönites from Kamarbon teschenite gabbro compositions in terms of ^{IV}Si–$^{VIII}(Na + K)$ and $^{VI}Ti^{+4}$ within the sapphirine group classification diagram together with the end member composition and compositional areas of analyzed phases (Grew et al. 2008)

and 20 oxygens and the Fe^{+2} and Fe^{+3} values are calculated by the Droop method (Droop 1987). The chemical composition of rhönites in teschenitic gabbro is as follows:

$$(Na, Ca)_{1.97}(Ti, {}^{VI}Al, Fe^{+3}, Fe^{+2}, Mn, Mg)_{5.99}(Si, {}^{IV}Al)_{6.02}O_{20}$$

The calculated Mg/(Mg + Fe^{+2}) values for Kamarbon rhönites range between 0.51 and 0.63. Figure 5 displays classification diagram for sapphirine group minerals that all analyzed Kamarbon rhönite samples fall in the rhönite field in this diagram.

Composition of rhönites in teschenitic gabbros is represented in diagrams $^{VIII}(Na + K) + {}^{IV}Si$ versus $^{VIII}Ca + {}^{IV}Al$ (Fig. 6a) (Babkine et al. 1964) and $^{IV}Fe^{+3}$ versus ($^{VI}Ti + Fe^{+2} + Mg$) (Fig. 6b) (Cameron et al. 1970). These diagrams highlight the occurrence of following exchange reactions respectively:

$$^{IV}Si^{+4} + {}^{VIII}(Na + K)^{+} \leftrightarrow {}^{IV}Al^{+3} + {}^{VIII}Ca^{+2}$$
$$^{VI}(Fe + Mg)^{+2} + Ti^{+4} \leftrightarrow {}^{VI}2Fe^{+3}$$

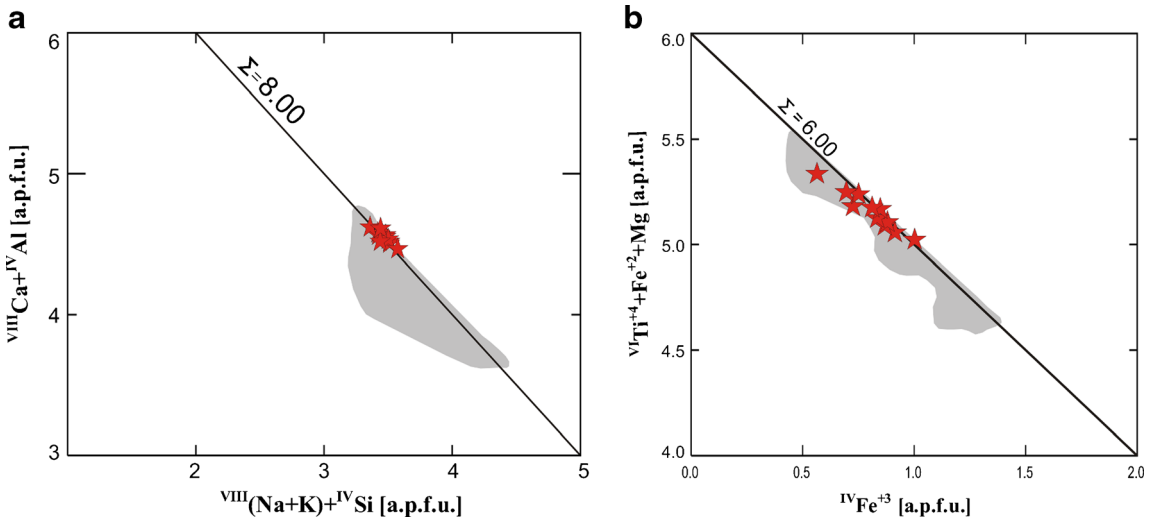

Fig. 6 **a** Plot of rhönites from Kamarbon teschenite gabbro in the Na + ^{IV}Si versus Ca + ^{IV}Al diagram (Babkine et al. 1964) and **b** $^{IV}Fe^{+3}$ versus ($^{VI}Ti + Fe^{+2} + Mg$) diagram (Cameron et al. 1970). The *gray field* is the representative composition of rhönites in igneous rocks (Grapes et al. 2003). In (**a**), analyses that deviate from the line = 8.00 contain appreciable Fe^{+3}; in (**b**), analyses that deviate from the line = 6.00 contain appreciable ^{IV}Al (and Cr^{+3})

The gray field in Fig. 6 is the typical mineralogical composition of rhönite in volcanic rocks (Grapes et al. 2003). In Fig. 7, almost all analysis of Kamarbon gabbros fall in the rhönite compositional field, which highlights the $Fe^{+2} \leftrightarrow Mg$ exchange reaction (Babkine et al. 1964).

Pyroxene

Chemical analyses of pyroxenes are represented in Table 2. Pyroxenes from theralite and teschenite are almost same in chemical composition. In the pyroxene classification diagram (Morimoto et al. 1988) most of the analyses plot above the diopside field (Fig. 8). Pyroxenes of theralites reveal higher Mg# (Mg/(Mg + Fe^{+2})) (from 92.1 to 73.6) than those of teschenities (from 90.1 to 60.5). The chemical composition of pyroxenes in theralites ranges from $Wo_{50}Fs_{10}En_{40}$ at core to $Wo_{53}Fs_{14}En_{34}$ at rim and in teschenites from $Wo_{51}Fs_{12}En_{37}$ at core to $Wo_{48}Fs_{22}En_{30}$ at rim. All pyroxenes represent low amount of SiO_2 and $Al_{total}/Ti < 10$.

Feldespatoid

The Kamarbon gabbro comprises nepheline and analcime as feldespatoid minerals. Nepheline is one of the main minerals in theralites whereas analcime is observed as one of the main minerals in teschenites. Both nephelines and analcimes are crystallized interstitially among olivine, pyroxene and plagioclase grains. Nephelines have Na_2O, 14.22–15.74 wt.%, K_2O, 3.74–4.86 wt.%, and Al_2O_3, 33.06–35.13 wt.%, and analcimes have Na_2O, 10.17–11.68 wt.%, K_2O, 0.01–0.10 wt.%, and Al_2O_3, 24.83–29.63 wt.%. Analcime is main mineral in teschenites which could be produced by magma crystallization and reveal primary composition like nephelines or might be secondary and produced by the alteration of nephelines (Morata and Higueras 1996).

Plagioclase

The composition of plagioclases in theralites varies from ($An_{59.16}$ $Ab_{39.34}$ $Or_{1.51}$) at core to ($An_{49.47}$ $Ab_{46.94}$ $Or_{3.59}$) at rim and in teschenites ranges from ($An_{46.81}$ $Ab_{49.69}$ $Or_{3.50}$) at core to ($An_{39.86}$ $Ab_{55.56}$ $Or_{4.58}$) at rim. Plagioclases from teschenites have higher Na content and represent andesinic composition, with those from theralites falling commonly in the labradorite field. A positive correlation is observed between the anorthite content in plagioclases and Mg# (Mg/(Mg + Fe^{+2})) in host rock. Some of plagioclases have undergone alteration to secondary minerals like sericite, clay, albite, and zeolite which shows increment from theralites toward teschenites.

Olivine

Olivine is the most abundant mineral in theralites and ranges from Fo_{84} at cores to Fo_{68} at rims. The chemical analyses of olivines are represented in Table 3. CaO ranges from 0.23 to 0.47 in olivines without large variations. Also in some teschenite gabbros, olivines are observed as accessory minerals.

Whole rock geochemistry

Chemical analyses of theralite and teschenite gabbros are presented in Table 4. In the QAPF classification diagram for plutonic rocks (Streckeisen 1974), most of the analyzed

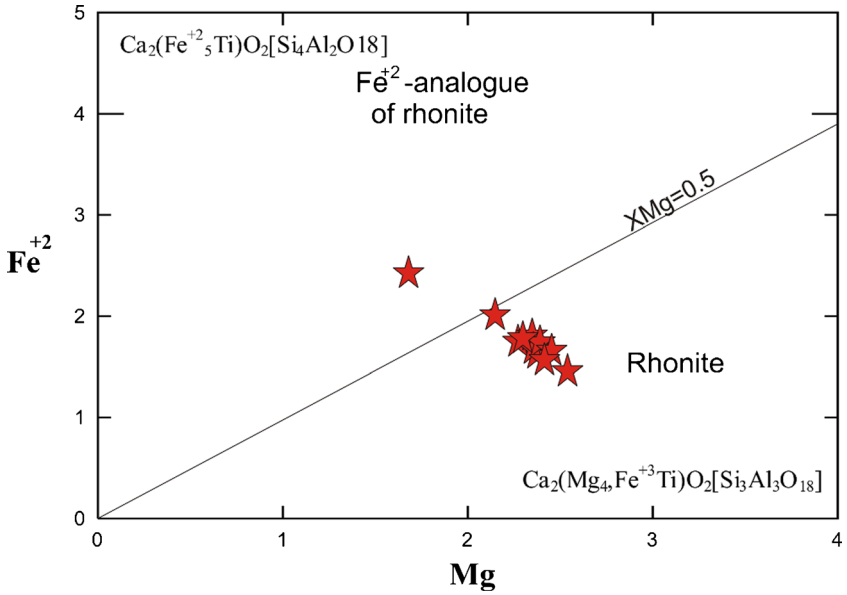

Fig. 7 Plot of rhönites in Mg versus Fe^{+2} diagram from Kamarbon teschenitic gabbro (Babkine et al. 1964)

Table 2 Microprobe analysis of pyroxenes in Kamarbon theralitic and teschenitic gabbro

Sample	RD182	RD182	RD182	RD182	RD182	RD182	RD172	RD172	RD172	RD172	RD172	RD181	RD181	RD181	RD181	RD181	RD181	RD181	RD181
Rock type																			
	Tes	Tes	Tes	Tes	Tes	Tes	Tes	Tes	Tes	Tes	Tes	Th	Th	Th	Th	Th	Th	Th	Th
Note																			
	Rim	Core	Rim	Middle	Core	Rim	Rim	Middle	Rim	Core	Core	Rim	Core	Middle	Rim	Middle	Core	Middle	Rim
SiO_2	47.74	46.50	46.16	45.43	41.83	41.98	45.61	42.52	40.47	44.28	44.05	46.31	45.89	44.74	42.66	43.32	46.32	42.66	42.54
TiO_2	2.13	3.15	2.77	3.33	4.87	5.04	3.86	4.69	5.37	3.49	3.71	2.92	2.34	3.38	4.55	3.62	2.56	3.98	4.94
Al_2O_3	7.53	7.43	6.99	7.66	11.01	11.02	6.92	10.29	12.04	8.68	9.30	6.48	8.75	8.84	10.87	10.64	6.36	10.75	10.98
Cr_2O_3	bdl	0.02	0.05	bdl	bdl	0.03	bdl	0.04	0.03	0.02	0.03	0.02	0.28	0.15	0.03	0.13	0.15	0.21	0.01
FeO	11.27	7.14	10.04	8.82	7.17	7.88	10.27	7.67	7.48	6.55	6.63	9.57	5.94	6.37	7.46	6.82	6.62	6.52	7.20
MnO	0.33	0.15	0.23	0.21	0.07	0.18	0.25	0.15	0.12	0.11	0.13	0.21	0.11	0.12	0.13	0.13	0.09	0.09	0.13
MgO	9.04	11.97	10.23	10.63	10.51	9.97	10.18	10.32	10.30	12.24	11.87	10.72	13.07	12.11	10.58	11.40	13.54	11.20	10.13
CaO	20.08	23.28	22.48	22.87	22.82	22.76	22.34	22.69	23.10	23.13	23.25	22.42	22.74	23.27	23.04	23.37	23.23	23.36	23.35
Na_2O	1.36	0.52	0.57	0.56	0.51	0.49	0.63	0.59	0.51	0.46	0.44	0.67	0.49	0.41	0.50	0.41	0.40	0.46	0.58
K_2O	0.03	0.01	bdl	0.02	bdl	bdl	bdl	0.01	bdl	bdl	bdl	0.01	bdl	bdl	0.02	bdl	0.02	0.01	0.01
Total	99.51	100.17	99.51	99.54	98.79	99.35	100.08	99.56	98.99	99.41	98.96	99.33	99.62	99.39	99.84	99.85	99.29	99.23	99.86
Si	1.81	1.73	1.75	1.71	1.58	1.59	1.72	1.61	1.52	1.66	1.65	1.75	1.70	1.67	1.60	1.61	1.73	1.60	1.60
Ti	0.06	0.09	0.08	0.09	0.14	0.14	0.11	0.13	0.15	0.10	0.10	0.08	0.07	0.09	0.13	0.10	0.07	0.11	0.14
Al	0.34	0.33	0.31	0.34	0.49	0.49	0.31	0.46	0.53	0.38	0.41	0.29	0.38	0.39	0.48	0.47	0.28	0.48	0.49
Cr	0.00	0.00	0.00	0.00	0.00	0.00	0.00	0.00	0.00	0.00	0.00	0.00	0.01	bdl	bdl	bdl	bdl	0.01	bdl
Fe^{3+}	0.02	0.08	0.07	0.08	0.10	0.08	0.07	0.09	0.15	0.13	0.12	0.09	0.12	0.10	0.10	0.13	0.15	0.13	0.08
Fe^{2+}	0.33	0.15	0.25	0.20	0.13	0.17	0.25	0.15	0.09	0.08	0.09	0.22	0.07	0.10	0.13	0.09	0.06	0.08	0.14
Mn	0.01	0.00	0.00	0.00	0.00	0.01	0.01	0.00	0.00	0.00	0.00	0.01	bdl	bdl	bdl	bdl	bdl	bdl	bdl
Mg	0.51	0.66	0.58	0.60	0.59	0.56	0.57	0.58	0.58	0.68	0.66	0.61	0.72	0.67	0.59	0.63	0.75	0.63	0.57
Ca	0.82	0.93	0.91	0.92	0.93	0.92	0.90	0.92	0.93	0.93	0.93	0.91	0.90	0.93	0.93	0.93	0.93	0.94	0.94
Na	0.10	0.04	0.04	0.04	0.04	0.04	0.05	0.04	0.04	0.03	0.03	0.05	0.04	0.03	0.04	0.03	0.03	0.03	0.04
K	0.00	0.00	0.00	0.00	0.00	0.00	0.00	0.00	0.00	0.00	0.00	0.00	bdl	bdl	bdl	bdl	bdl	bdl	bdl
Total	4.00	4.00	4.00	4.00	4.00	4.00	4.00	4.00	4.00	4.00	4.00	4.00	4.00	4.00	4.00	4.00	4.00	4.00	4.00
Wo	48.15	51.02	50.25	51.15	52.96	53.03	49.96	52.58	53.27	50.98	51.62	49.85	49.82	51.49	52.73	52.34	49.11	52.96	54.09
En	30.14	36.51	31.81	33.08	33.92	32.31	31.67	33.28	33.05	37.56	36.66	33.17	39.83	37.29	33.71	35.52	39.81	35.33	32.65
Fs	21.71	12.47	17.94	15.77	13.12	14.66	18.37	14.14	13.68	11.46	11.71	16.98	10.35	11.22	13.57	12.14	11.07	11.70	13.26
N° Mg	60.53	81.95	70.13	75.14	82.51	76.90	69.26	79.68	86.83	90.11	88.03	73.60	91.45	87.40	81.60	88.11	92.91	89.05	79.90
P_1 (kbar)		0.5		0.7	0.9			1.1		1.8	1.2		4.5	2.2		3.8	3.0	3.7	
P_2 (kbar)		0.4		1.3	0.7			1.2		1.5	1.9		4.4	1.9		3.5	2.4	3.4	
P_3 (kbar)		0.6		1.1	0.8			1.4		1.3	1.0		4.3	1.8		3.3	2.6	3.2	

Calculation is based on 6 oxygens. (Th and Tes are symbols of theralitic and teschenitic gabbros)

samples fall in the feldespatoid gabbros and feldespatoid monzo gabbro fields (Fig. 9).

In Kamarbon gabbros, fine-grained theralites have lower Al_2O_3 (14.09 to 15.56 wt.%) and higher MgO (8.10 to 11.68 wt.%) with Mg# (64.21 to 71.39) content compared with coarse-grained teschenities (14.57 to 19.02 wt.%, 6.38 to 2.67 wt.%, and 43.22 to 57.2 for Al_2O_3, MgO, and Mg#, respectively). Most of the major elements in Kamarbon gabbroic rocks ranges in wild way (e.g., MgO ranging from ~12 to ~2 wt.%) not associated with substantial SiO_2 change in the residual melt.

Fine-grained theralitic gabbro shows more Ni, Cr, and Co content than teschenitic one. Ni of theralites and teschenites varies from 95 to 194 ppm and 7 to 67 ppm, respectively. Ni and Co show positive trend with increasing MgO whereas Nb and Ba show negative correlation. The Kamarbon intrusion is enriched in LREE respect to HREE with $(La/Yb)_N$ and $(Dy/Yb)_N$ ratios ranging from 20.00 to 29.73 and 1.39 to 1.68 for theralites and teschenites, respectively. The gabbroic rocks reveal the similar trend with OIB basalts and intraplate alkaline magmatism (Beccaluva et al. 2002; Bianchini et al. 2007; Beccaluva et al. 2009) (Fig. 10a). They show enrichment of LILE elements (Ba, Rb, Sr, and Th), HFSE elements (Nb, Ta, Ti, Zr, and Hf) and P and depletion in K, Y and HREE (Yb, Lu) (Fig. 10b).

Estimation the P-T of gabbro

Geothermobarometry calculations in gabbroic rocks can nearly distinct the equilibrium pressure and temperature that can lead us to understand the crystallization condition of intrusions. In Kamarbon gabbros, the composition of clinopyroxenes is used to estimate the equilibrium pressure while the olivine-liquid composition is applied to gain the equilibrium temperature.

According to the method of Nimis and Taylor (2000), the values of Cr, Na, and K in clinopyroxene composition can be use to determine the pressure. This barometer has lower temperature dependency than other barometers, which are based on Al content in pyroxene compositions. The clinopyroxene barometers of Nimis (1995) (P_1), Nimis and Ulmer (1998) (P_2), and Nimis and Taylor (2000) (P_3) are used, and the crystallization pressures are calculated on the basis of three relations. P_1, P_2, and P_3 range from 0.5 to 1.8 kbar, from 0.4 to 1.9 kbar, and from 0.6 to 1.4 kbar in teschenites, whereas in theralites, they change from 2.2 to 4.5 kbar, from 1.9 to 4.4 kbar, and from 1.8 to 4.3 kbar, respectively. The calculated pressures are reported in Table 2.

To obtain a reasonable crystallization temperature for the Kamarbon theralitic and teschenitic gabbros, the olivine-liquid thermometer from Sisson and Grove (1993) (T_1) are used (Table 3). Calculated temperatures based on olivine-liquid composition (T_1) range from 1067 to 1075 °C in teschenites, whereas they change from 1266 to 1270 °C in theralites.

Discussion

Crystallization and the stability field of rhönite

Several studies have tried to clear the formation condition of rhönite. Boivin (1980) believed that rhönite normally occurs below 1 kbar, at about 1100 to 1170 °C, accompanied by plagioclase. Experimental data of Kunzmann (1989) show

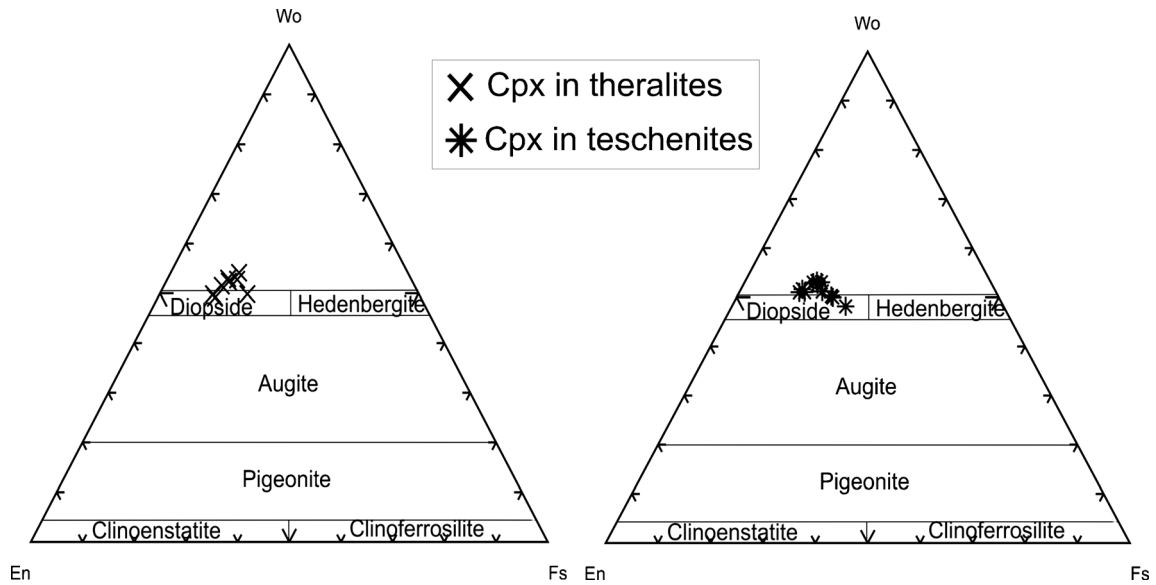

Fig. 8 Pyroxenes of Kamarbon theralite and teschenite gabbros in the classification ternary diagram of pyroxenes (Morimoto et al. 1988)

Table 3 Microprobe analysis of olivines in Kamarbon theralie and teschenite gabbros

Sample	RD181	RD181	RD181	RD181	RD181	RD181	RD181	RD172	RD172	RD172	RD172	RD172
Rock type	Th	Th	Th	Th	Th	Th	Th	Tes	Tes	Tes	Tes	Tes
Note	Rim	Middle	Core	Middle	Rim	Rim	Rim	Middle	Middle	Core	Middle	Rim
SiO_2	39.37	38.54	39.39	39.50	38.06	37.49	38.55	38.58	38.96	39.95	39.57	39.17
TiO_2	0.01	bdl	0.04	0.03	0.01	0.03	0.03	0.02	0.01	0.01	bdl	bdl
Al_2O_3	bdl	bdl	0.04	0.03	0.03	0.07	0.04	0.03	0.02	0.07	0.05	0.02
Cr_2O_3	0.02	0.03	0.02	0.02	0.01	0.01	0.02	0.01	0.02	0.03	0.03	bdl
FeO	17.27	20.89	15.52	16.24	24.30	27.73	22.98	21.28	16.81	15.54	17.21	17.96
MnO	0.27	0.46	0.26	0.22	0.52	0.61	0.46	0.44	0.32	0.22	0.31	0.30
MgO	43.82	41.10	45.76	45.06	37.85	34.42	39.03	40.28	46.68	45.66	44.35	43.46
CaO	0.32	0.36	0.26	0.28	0.47	0.51	0.40	0.38	0.25	0.25	0.23	0.25
Na_2O	0.04	bdl	0.01	0.01	0.01	bdl	bdl	0.02	bdl	bdl	0.02	0.01
Total	101.12	101.54	101.30	101.39	101.26	100.89	101.52	101.29	103.06	101.74	101.77	101.44
Si	0.99	0.98	0.98	0.99	0.99	0.99	0.99	0.99	0.96	0.99	0.99	0.99
Ti	0.00	0.00	0.00	0.00	0.00	0.00	0.00	0.00	0.00	0.00	0.00	0.00
Al	0.00	0.00	0.00	0.00	0.00	0.00	0.00	0.00	0.00	0.00	0.00	0.00
Cr	0.00	0.00	0.00	0.00	0.00	0.00	0.00	0.00	0.00	0.00	0.00	0.00
Fe^{2+}	0.36	0.45	0.32	0.34	0.53	0.62	0.49	0.46	0.35	0.32	0.36	0.38
Mn	0.01	0.01	0.01	0.00	0.01	0.01	0.01	0.01	0.01	0.00	0.01	0.01
Mg	1.64	1.56	1.70	1.68	1.47	1.36	1.50	1.54	1.72	1.68	1.65	1.63
Ca	0.01	0.01	0.01	0.01	0.01	0.01	0.01	0.01	0.01	0.01	0.01	0.01
Na	0.00	0.00	0.00	0.00	0.00	0.00	0.00	0.00	0.00	0.00	0.00	0.00
Total	3.01	3.02	3.02	3.01	3.01	3.00	3.01	3.01	3.04	3.01	3.01	3.01
Fo	81.66	77.43	83.79	82.99	73.10	68.40	74.79	76.77	82.93	83.77	81.86	80.92
Fa	18.05	22.08	15.94	16.78	26.33	30.91	24.71	22.75	16.75	16.00	17.82	18.76
N° Mg	81.90	77.81	84.01	83.18	73.52	68.87	75.17	77.14	83.20	83.96	82.12	81.18
T_1 °C		1270	1266	1269				1077	1067	1069	1073	

Calculation is based on 4 oxygens. (Th and Tes are symbols of theralitic and teschenitic gabbros)

that the formation of rhönite under magmatic conditions requires pressures below 0.6 kbar and temperature between 840 to 1200 °C, with the presence of hydrous liquid phase. But some authors (Kóthay and Szabó 1999; Nazarov et al. 2000; Kóthay et al. 2001; Sharygin et al. 2003) believe that rhönite can form at rather higher pressure and temperature conditions, as a primary phase.

The values of MgO and Ni in theralites are compatible with the definition of primitive magmas, according to Frey et al. (1978; Mg# >68). On the other hand, MgO, Ni, and Mg# values in teschenites are much lower. The positive trends between Ni, Cr, Co, and MgO in Kamarbon gabbroic rocks could imply the fractionation of minerals like olivine and pyroxene. Theralites can be considered primitive magma parental to the teschenites after fractional crystallization of mafic phases like olivine and clinopyroxene. The crystallization process in Kamarbon gabbros also can be confirmed by the mineralogical assemblage of olivine + clinopyroxene + nepheline + plagioclase in theralites and clinopyroxene + rhönite + analcime + plagioclase in teschenites (Doroozi 2014).

Clinopyroxene and olivine geothermobarometry calculations of Kamarbon gabbroic rocks reveal that the theralites are crystallized at higher pressures and temperatures than teschenites. Clinopyroxene barometry in teschenites suggests $P < 1.9$ kbar (0.4 to 1.9 kbar, corresponding to a depth range of about 6–10 km), whereas in theralites, this value is $P < 4.5$ kbar (1.8 to 4.5 kbar, corresponding to a depth range of about 10–18 km). The temperatures calculated from olivine-liquid thermometer for teschenites (1067 to 1075 °C) are lower than those of theralites (1266 to 1270 °C). Based on geothermobarometry calculations, rhönite could be crystallized in Kamarbon teschenites, in pressures less than 1.9 kbar (corresponding to a depth less than 10 km) and temperatures from 1067 to 1075 °C. These pressures and temperatures are

Table 4 XRF and ICP analysis of Kamarbon theralite and teschenite gabbroic rocks

Sample	RD176C	RD177C	RD178C	RD179C	RD178F	RD181F	RD170	RD182C	RD300C	RD167C	RD168C	RD171C
	Rock type											
	Teschenite	Teschenite	Teschenite	Teschenite	Theralite	Theralite	Theralite	Teschenite	Teschenite	Teschenite	Teschenite	Teschenite
SiO_2	47.04	44.21	44.41	47.62	45.42	44.41	44.79	45.86	46.74	46.95	46.89	40.00
TiO_2	2.40	2.90	2.97	2.30	2.14	2.06	2.13	2.59	2.41	2.26	2.37	3.91
Al_2O_2	18.90	16.75	16.67	19.04	15.56	14.09	14.79	17.15	18.32	18.46	18.58	14.57
Fe_2O_3	7.07	8.43	8.25	6.65	8.95	9.57	9.42	8.63	8.42	6.40	8.32	9.53
MnO	0.15	0.14	0.14	0.15	0.17	0.17	0.16	0.16	0.15	0.15	0.16	0.12
MgO	2.82	5.10	4.47	2.63	8.10	11.68	10.63	3.90	3.65	2.93	3.21	6.38
CaO	9.25	11.62	12.50	9.18	11.13	11.01	11.04	9.93	9.49	9.58	9.64	14.05
Na_2O	8.75	6.97	7.13	8.70	6.03	4.68	4.94	7.20	6.97	9.08	7.58	7.49
K_2O	1.95	1.76	1.46	2.08	1.41	1.40	1.16	2.85	2.23	2.37	1.82	1.16
P_2O_5	1.63	2.07	1.95	1.60	1.04	0.88	0.89	1.69	1.58	1.78	1.37	3.20
Total	99.96	99.95	99.95	99.95	99.95	99.95	99.95	99.96	99.96	99.96	99.94	99.94
L.O.I	1.3	2.0	2.2	3.4	2.1	2.1	1.9	3.1	4.1	3.1	4.2	2.1
Ba	2438	1660	1838	2463	1576	1065	1282	1575	1926	2126	1948	1233
Co	26.10	32.30	30.20	23.90	45.30	51.70	58.50	28.80	24.80	23.80	33.10	34.10
Cr	3.00	27.00	16.40	0.30	317.50	448.30	416.20	5.10	0.20	2.10	2.80	26.50
Cu	97.90	56.10	68.30	87.50	65.10	48.40	56.10	77.10	91.10	84.90	94.50	66.50
Ga	16.30	16.30	18.10	16.40	12.20	12.30	13.10	17.30	15.80	16.80	17.30	27.60
Hf	5.00	3.30	2.90	4.70	4.10	3.50	3.60	4.20	5.20	4.00	6.40	0.10
Nb	146	103	113	143	99.80	80.20	86.20	146.30	134.10	133.00	157.70	110.50
Nd	83.00	95.50	100.60	84.80	56.00	39.70	45.40	89.90	83.00	84.50	73.40	159.70
Ni	8.00	31.30	25.60	7.40	94.50	176.00	155.30	19.40	12.50	7.40	6.40	67.40
Rb	30.50	23.30	17.20	31.00	17.70	13.30	9.30	85.20	21.10	29.20	23.20	19.10
Sc	0.00	4.10	4.70	0.00	13.70	22.00	21.10	1.60	0.30	0.00	0.00	3.80
Sr	1915	1958	1685	1632	1387	1145.	1134	874	2098	1426	2331	1456
Th	9.09	6.68	7.53	9.42	7.27	5.57	5.57	9.55	8.12	8.05	9.68	4.27
V	195	284	315	192	229.60	216.90	219.90	233.50	186.30	190.10	178.50	383.60
Y	24.33	23.28	25.67	23.76	23.09	23.37	23.37	26.15	22.80	21.36	25.38	21.65
Zn	64.00	50.90	55.10	60.50	63.70	53.60	54.00	68.20	63.20	56.00	70.70	46.70
Zr	240	229	253	226	200.40	186.50	192.70	238.10	228.20	208.80	256.20	246.70
Ce			133.52		91.38	81.95		139.09		127.57		147.98
Pr			13.64		9.19	8.55		13.41		12.34		15.05
Sm			8.85		5.93	5.71		7.99		7.19		9.06
Eu			2.77		1.97	1.85		2.52		2.41		2.62
Gd			8.22		5.54	5.34		7.40		6.83		8.32
Tb			1.17		0.79	0.78		1.02		0.96		1.14
Dy			5.24		3.48	3.50		4.51		4.28		4.91
Ho			1.01		0.67	0.67		0.86		0.84		0.93
Er			2.59		1.72	1.71		2.26		2.23		2.36
Tm			0.38		0.25	0.25		0.33		0.34		0.34
Yb			2.17		1.46	1.47		1.94		2.01		1.91
Lu			0.32		0.21	0.21		0.28		0.29		0.28
Hf			3.98		3.33	3.33		3.51		2.85		3.40

Table 4 (continued)

Sample	RD176C	RD177C	RD178C	RD179C	RD178F	RD181F	RD170	RD182C	RD300C	RD167C	RD168C	RD171C
Rock type	Teschenite	Teschenite	Teschenite	Teschenite	Theralite	Theralite	Theralite	Teschenite	Teschenite	Teschenite	Teschenite	Teschenite
Ta			6.20		4.70	4.21		8.91		6.88		5.97
U			2.14		1.88	1.49		2.73		2.59		1.99

Sample	RD172C	RD165F	RD166F	RD169F	RD170F	RD171F	RD173F	RD174F	RD175F	RD177F
Rock type	Teschenite	Theralite	Theralite	Theralite	Theralite	Theralite	Theralite	Theralite	Theralite	Theralite
SiO_2	44.40	44.35	44.76	44.78	44.95	44.56	44.68	44.64	44.48	45.05
TiO_2	3.14	2.04	2.08	2.11	2.12	2.00	2.11	2.10	2.14	2.10
Al_2O_2	16.10	14.26	14.68	14.31	14.75	14.39	15.38	15.06	14.24	14.70
Fe_2O_3	7.39	9.40	8.71	9.32	9.15	9.33	8.95	9.01	8.94	10.40
MnO	0.12	0.17	0.17	0.17	0.16	0.17	0.16	0.17	0.17	0.17
MgO	4.41	11.49	10.50	10.72	10.63	10.98	9.63	9.74	11.25	10.32
CaO	12.18	11.05	11.27	11.06	11.13	11.04	11.41	11.30	11.33	10.99
Na_2O	8.44	4.89	5.60	5.01	5.02	5.17	5.36	5.69	5.39	4.13
K_2O	1.55	1.42	1.33	1.62	1.14	1.37	1.35	1.30	1.23	1.34
P_2O_5	2.21	0.86	0.89	0.87	0.90	0.93	0.93	0.94	0.80	0.76
Total	99.94	99.93	99.99	99.97	99.95	99.94	99.96	99.95	99.7	99.96
L.O.I	3.1	1.9	1.5	1.9	3.0	3.2	3.1	2.1	1.9	1.2
Ba	1492	932	962	959	1245	1143	1058	1077	1011	1266
Co	30.90	54.20	52.60	50.00	50.30	45.80	49.50	50.40	54.80	57.60
Cr	18.70	504.50	569.70	520.80	424.10	407.30	439.90	439.20	533.10	418.40
Cu	61.50	50.00	53.40	53.40	55.60	48.60	56.40	61.80	49.90	53.90
Ga	21.20	11.70	12.20	11.10	13.10	11.90	11.70	12.30	10.90	11.20
Hf	2.40	3.50	3.20	3.10	4.00	3.60	3.60	3.50	3.50	4.00
Nb	135.20	74.90	79.40	82.40	79.90	83.60	82.10	77.10	76.60	80.20
Nd	111.10	42.30	46.80	43.60	46.00	39.50	46.80	47.30	46.40	40.00
Ni	29.50	193.60	175.10	177.30	153.30	152.40	145.60	140.80	172.40	184.00
Rb	26.70	14.50	13.10	25.50	9.90	20.30	10.80	14.20	13.70	17.30
Sc	3.70	26.70	21.90	20.50	20.90	17.50	19.50	19.60	26.50	25.50
Sr	1195	951	840	807	1085	1031	1068	946	930	1206
Th	7.92	5.96	5.70	6.61	6.22	5.38	6.29	5.96	6.55	5.90
V	327.60	216.70	234.60	237.30	225.20	210.40	231.10	230.10	242.20	231.50

Table 4 (continued)

Sample	RD172C Rock type	RD165F	RD166F	RD169F	RD170F	RD171F	RD173F	RD174F	RD175F	RD177F
	Teschenite	Theralite	Theralite	Theralite	Theralite	Theralite	Theralite	Theralite	Theralite	Theralite
Y	25.19	22.90	22.61	23.76	22.80	22.70	23.47	22.99	23.85	22.61
Zn	48.60	55.10	59.10	57.80	54.70	53.80	56.70	58.90	56.80	63.40
Zr	262.00	173.70	179.80	181.70	175.80	180.90	186.60	179.00	178.70	188.60
Ce	134.86	77.27		82.87					78.22	
Pr	13.22	8.29		8.70					8.23	
Sm	8.26	5.56		5.82					5.48	
Eu	2.50	1.78		1.86					1.77	
Gd	7.68	5.14		5.46					5.14	
Tb	1.08	0.76		0.81					0.76	
Dy	4.86	3.43		3.65					3.42	
Ho	0.94	0.65		0.71					0.66	
Er	2.46	1.69		1.83					1.71	
Tm	0.37	0.25		0.27					0.25	
Yb	2.16	1.45		1.55					1.45	
Lu	0.32	0.21		0.23					0.21	
Hf	3.49	3.25		3.28					3.22	
Ta	6.56	4.06		4.14					4.27	
U	2.41	1.53		1.50					1.52	

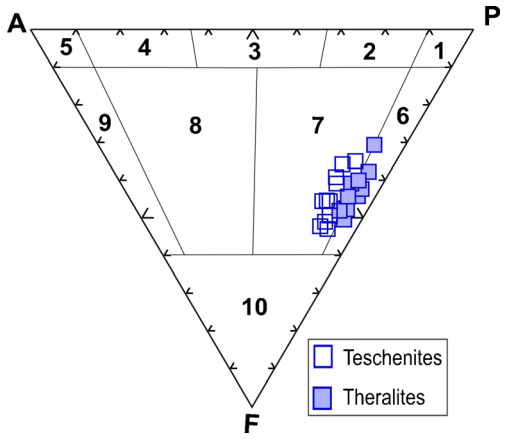

Fig. 9 Samples from Kamarbon theralite and teschenite gabbros plot in QAPF diagram for classification of plutonic rocks (Streckeisen 1974). (*1*, Foid-bearing diorite, Foid-bearing gabbro; *2*, Foid-bearing diorite; *3*, Foid-bearing monzonite; *4*, Foid-bearing syenite; *5*, Foid-bearing alkali feldspar syenite; *6*, Foid gabbro; *7*, Foid monzodiorite; *8*, Foid monzosyenite; *9*, Foid syenite; *10*, Foidolite)

partly compatible with previous published data about stability field and crystallization condition of rhönite (Kóthay and Szabó 1999; Nazarov et al. 2000; Kóthay et al. 2001; Sharygin et al. 2003). The formation of theralitic gabbros exactly at higher pressures and temperatures than teschenitic ones, could suppress rhönite crystallization in theralites. Rhönite formation in Kamarbon teschenites can be regarded as the products of late stage of crystallization at shallow depth corresponding to a depth of about 6–10 km.

Important factors of the rhönite crystallization can be the high Al, rather low Ca, and low Si contents in undersaturated magmas. The average values of TiO_2 and CaO in Kamarbon teschenites are 2.70 and 15.76 wt.% respectively, while the corresponding values in theralites are 2.00 and 11.10 wt.%. Magonthier and Velde (1976) believed that the rhönite is a Ti-enriched mineral that its crystallization could not be caused by high amounts of Ti in magma. However, other studies suggest that the TiO_2 > 2.5 wt.% in alkaline magmas can play an important role in the rhönite crystallization (Boivin 1980; Nedli and Toth 2003). Accordingly, the crystallization of rhönite in Kamarbon teschenites can be related to the higher amount of TiO_2 and CaO in teschenites rather than theralites.

Genesis of rhönite and associated minerals

The Kamarbon teschenitic gabbros mineralogical composition is clinopyroxene, rhönite, plagioclase, and analcime. The chemically undersaturated magmas usually are accompanied by minerals like analcime, nepheline, and rhönite. The diopsidic clinopyroxenes of teschenites exhibit the characters of clinopyroxenes in alkaline basic magmas, i.e., they are enriched in Al_2O_3 and TiO_2 and depleted of silica (Table 2). The low Si content in clinopyroxenes of teschenitic gabbros may be caused by the low content of Si in its undersaturated parental magma (Magonthier and Velde 1976; Onuma 1983; Anan'ev and Selyangin 2011). Studies on associated minerals of the rhönite reveal that there is a stable paragenesis between rhönite and Al-rich clinopyroxene, while other minerals like

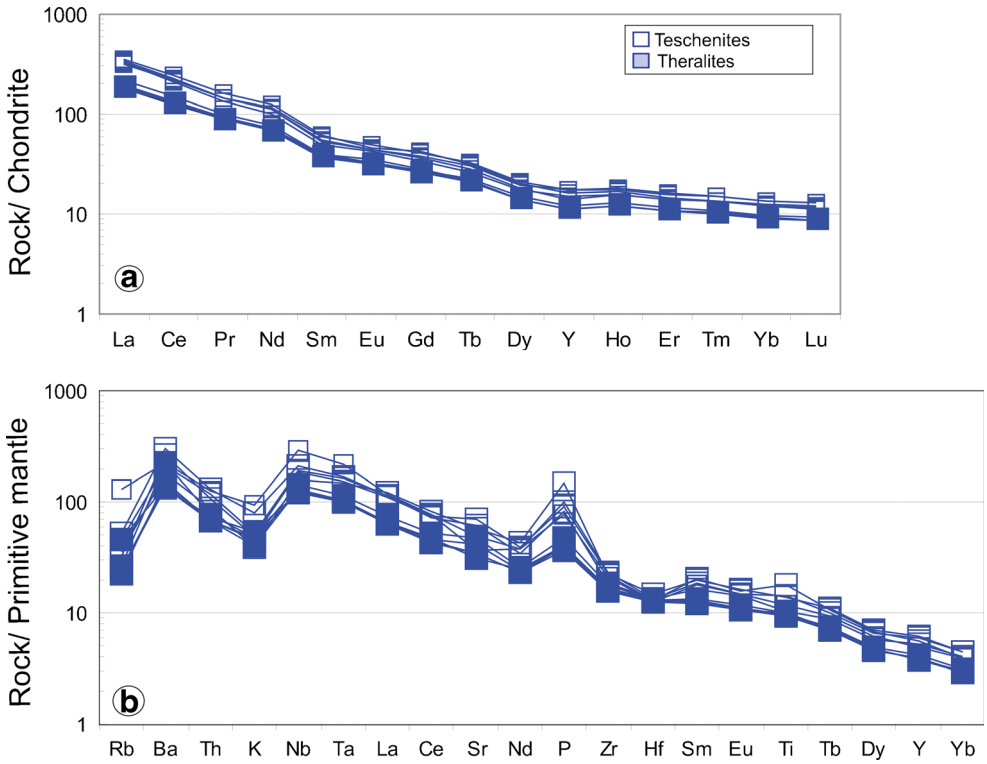

Fig. 10 **a** Chondrite-normalized diagram for Kamarbon gabbroic rocks; normalized values are from Nakamura (1974). **b** Primitive mantle-normalized diagram for Kamarbon rocks; normalized values are from McDonough and Sun (1995)

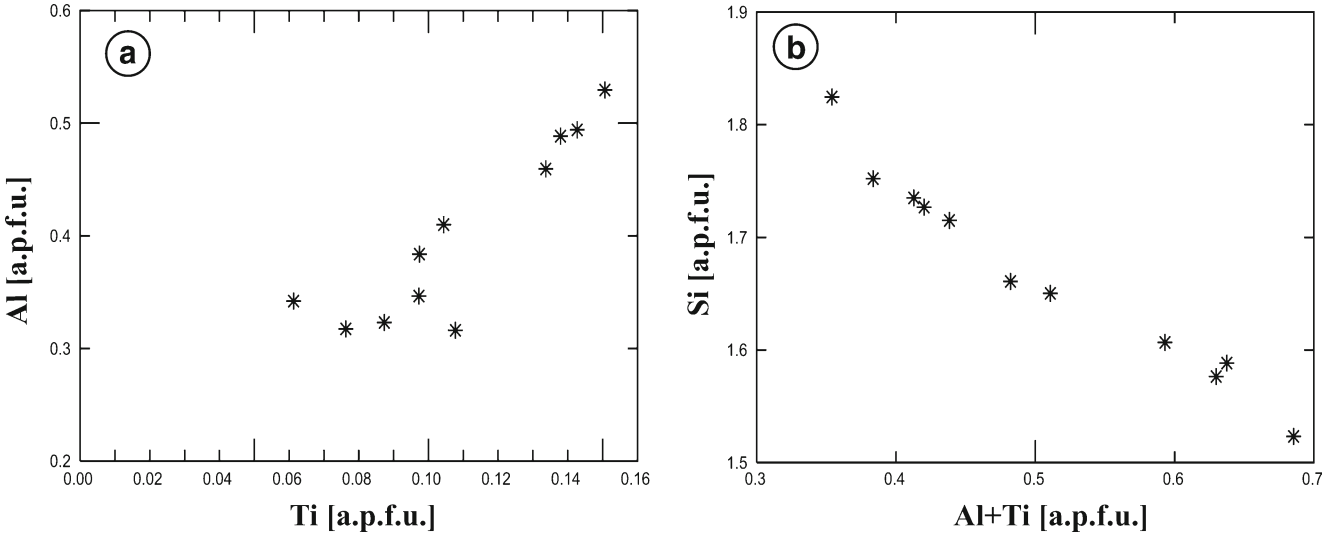

Fig. 11 **a** Plot of Ti versus Al and **b** Al + Ti versus Si in clinopyroxenes of Kamarbon teschenite gabbro

olivine, amphibole, nepheline, analcime, and leucite could be variable (Soellner 1907; Magonthier and Velde 1976; Fodor and Hanan 2000; Sharygin 2002; Kogarko et al. 2005; Timina et al. 2006; Anan'ev and Selyangin 2011). Clinopyroxenes of teschenitic gabbros become more enriched of Ti and Al during the fractional crystallization process which involves enrichment in Al and Ti and depletion of Si of magma (Fig. 11).

Rhönite can be a primary or a secondary mineral produced by alteration of kaersutite (Magonthier and Velde 1976; Johnston and Stout 1985). High values of Na + ^{IV}Si and low values of Ca + ^{IV}Al are the characteristics of the rhönites produced by alteration of kaersutite, whereas the primary rhönites reveal low Na + ^{IV}Si and high Ca + ^{IV}Al (Nedli and Toth 2003). The composition of the rhönites in teschenitic gabbros in comparison with that of the rhönites in igneous rocks (gray field in Fig. 6a) show lower Na + ^{IV}Si and higher Ca + ^{IV}Al, which can be a sign of primary rhönites. Crystallization of primary rhönite is related to the composition of parental magma and acted independently of unusual temperatures, oxygen fugacity, or the unusual physical crystallization conditions (Kyle and Price 1975).

Huckenholz et al. (1988) suggested that in ascending magma, the prior crystallized kaersutites will lose their stability and breakdown into a rhönite + plagioclase mineral assemblage, at low pressure and relatively high temperature ($P < 0.5$ kbar and 1050 °C < T < 1140 °C). Regarding the higher-pressure formation of Kamarbon teschenites (0.4 to 1.9 kbar), the crystallized rhönites can reveal primary igneous origin and crystallization at shallow depth (6 to 10 km) (Nedli and Toth 2003).

Conclusion

The Late Triassic to Upper Jurassic Kamarbon gabbro comprises theralites at margins and teschenites at center with the occurrence of rhönite in teschenitic gabbros. Mineralogically, teschenitic gabbros contain clinopyroxene, rhönite, plagioclase, and analcime plus accessory minerals. High $(La/Yb)_N$ in Kamarbon gabbroic rocks suggests a lower degree of partial melting in their mantle source. The $(Dy/Yb)_N > 1.06$ ratio in studied gabbros, signifies the presence of garnet as a residual phase during the partial melting (Blundy et al. 1998; Peters et al. 2008). Based on geochemical characteristics, theralites can be considered primitive magmas parental to the teschenitic gabbros after fractional crystallization of mafic phases like olivine and clinopyroxene. Based on the petrographical observations and estimating the formation pressure and temperature of Kamarbon gabbros, the teschenites were formed in distinctive lower pressures and temperatures than theralites. Experimentally obtained data indicate that the teschenites formed below 1.9 kbar and 1075 °C (based on clinopyroxene and olivine thermobarometry). Rhönites probably formed in teschenites in the late stage of crystallization at shallow depth which is about 6–10 km.

The exchange reaction $^{IV}Si^{+4} + {}^{VIII}(Na + K)^{+} \leftrightarrow {}^{IV}Al^{+3} + {}^{VIII}Ca^{+2}$ that occurred in Kamarbon rhönites caused higher values of Ca + ^{IV}Al, which is a sign of primary rhönite compositions. The former amphiboles can lose their stability and convert into rhönite and plagioclase assemblage at the $P < 0.5$ kbar and 1050 °C < T < 1140 °C. Based on the determined higher-pressure formation for Kamarbon teschenites (0.4 to 1.9 kbar), the crystallized rhönites can reveal primary igneous origin in Kamarbon gabbros.

Mineralogical and chemical characteristics of rhönite and associated minerals signify the formation of rhönite from Al- and Ti-enriched undersaturated alkaline magma in Kamarbon gabbroic intrusion. The rhönite observed in teschenitic gabbros illustrates the existence of an undersaturated plutonism phase, in Alpine-Himalayan orogenic belt, during the Late Triassic to Upper Jurassic in Central Alborz, north Iran. This alkaline magmatic phase can be assumed as an

evidence for intracontinental tectonic setting related to a rift system in Central Alborz during the Late Triassic. The extensional phases developed some regional rifts which caused volcanism and plutonism activities in Central Alborz.

References

Alavi M (1991) Sedimentary and structural characteristics of the Paleo-Tethys remnants in northeastern Iran. Geological Society of America, Bulltin 103:983–992

Alavi M (1996) Tectonostratigraphic sunthesis and structural style of the Alborz mountain system in northern Iran. J Geodyn 33:1–21

Anan'ev VV, Selyangin OB (2011) Rhönite molten inclusions from the olivine of aliivalite nodules from Malyi Semyachik volcano and basalts of Klychevskoi volcano, Kamchatca. J Volcanol Seismol 5: 355–340

Annels RN, Arturton RS, Bazley RAB, Davis, RC with contribution of Hamedi M, Rahimzahed F, Rashtian K (1985) Explanatory text of the Qazvin and Rasht quadrangle map. Geological Survey of Iran, Tehran, Iran

Ansari M, Vossoughi Abedini M, Darvish Zadeh A, Sheikhzakariaee SJ, Hossein Mirzaee Beni Z (2011) Geochemical constrain on the Early Cretaceous, OIB-type alkaline volcanic rocks in Kojor volcanic field, Central Alborz Mountain, north of Iran. Aust J Basic Appl Sci 10:913–925

Babkine JF, Conquéré JC, Duong PK (1964) Sur un nouveau gisement de rhönite (Monistrol d'Allier, Haute Loire). Cr Acad Sci 258:5479–5481

Beccaluva L, Coltorti M, Di Girolamo P, Melluso L, Milan L, Morra V, Siena F (2002) Petrogenesis and evolution of Mt. Vulture alkaline volcanism (southern Italy. Mineral Petrol 74:277–297

Beccaluva L, Bianchini G, Natali C, Siena F (2009) Continental flood basalts and mantle plumes: a case study of the northern Ethiopian plateau. J Petrol 50:1377–1403

Berberian M (1983) The southern Caspian: a compressional depression floored by a trapped, modified oceanic crust. Can J Earth Sci 20: 163–183

Berberian M, King GCP (1981) Towards a paleogeography and tectonic evolution of Iran. Can J Earth Sci 18:210–265

Bianchini G, Beccaluva L, Siena F (2007) Post-collisional and intraplate Cenozoic volcanism in the rifted Apennines/Adriatic domain. Lithos 101:125–140

Blundy JD, Robinson JAC, Wood BJ (1998) Heavy REE are compatible in clinopyroxene on the spinel lherzolite solidus. Earth Planet Sci Lett 160:493–504

Boivin P (1980) Données experimentales préliminaires sur la stabilité de la rhönite a'1 atmosphere. Application aux gisements naturels. B Mineral 103:491–502

Bonaccorsi E, Merlino S, Pasero M (1990) Rhönite: structural and microstructural features, crystal chemistry and polysomatic relationships. Eur J Mineral 2:203–218

Brooks CK, Pedersen AK, Rex DC (1979) The petrology and age of alkaline mafic lavas from the nunatak zone of central East Greenland. Grønlands Geologiske Undersøegelse Bullten 133:1–28

Brunet MF, Korateav MW, Arshov AV, Nikishin AM (2003) The South Caspian Basin: a review of its evolution from subsidence modeling. Sediment Geol 148:119–156

Cameron KL, Carman MF, Butler JC (1970) Rhönite from big bend National Park, Texas. Am Mineral 55:864–874

Cartier EG (1971) Geology of the lower Chalus Valley, central Alborz, Iran. Geological institute, ETH-Zurich, pp. 1–164

Deer WA, Howie RA, Zussman J (1978) Rock-forming minerals. Vol.2a, single chain silicates. Wiley, New York

Dostal J, Owen JV (1998) Cretaceous alkaline lamprophyres from north-eastern Czech Republic: geochemistry and petrogenesis. Int J Earth Sci 87:67–77

Droop TR (1987) A general equation for estimating Fe^{3+} concentration in feromagnesian silicates and oxides from microprobe analysis, using stoichiometric criteria. Mineral Mag 51:431–435

Fauvelet F, Eftekhar Nezhad J (1992) Explanatory text of the Gonbad quadrangle map (1/250000). Geological Survey of Iran, Tehran

Fodor RV, Hanan B (2000) Geochemical evidence for the Trinidade hotspot trace: Columbia seamount ankaramite. Lithos 51:293–304

Franzini M, Leoni L, Saitta M (1975) Revisione di una metodologia analitica per fluorescenza-X basata sulla correzione completa degli effetti di matrice. Rend Soc Ital Mineral Petrol 31:365–378

Frey FA, Green DH, Roy SD (1978) Integrated models of basalt petrogenesis: a study of quartz tholeiites to olivine melilitites from south eastern Australia utilizing geochemical and experimental petrological data. J Petrol 19:463–513

Furon R (1941) Géologie du plateau iranien (Perse-Afghanistan-Beloutchistan). Paris, Mém Mus Nal Hist Natur 7:414–177

Grapes RH, Wysoczanski RJ, Hoskin PWO (2003) Rhönite paragenesis in pyroxenite xenoliths, Mount Sidley volcano, Marie Byrd Land, West Antarctica. Mineral Mag 67:629–651

Grew ES, Halenius U, Pasero M, Barbier J (2008) Recommended nomenclature for the sapphrine and surinamite groups (sapphirine supergroup. Mineral Mag 72:839–876

Grünhagen H, Seck HA (1972) Rhönite aus einem Metaphonolith vom Puy de Saint-Sandoux (Auvergne). Swiss Bulletin of Mineralogy and Petrology 18:17–38

Guest B, Axen GJ, Lam PS, Hassanzadeh J (2006) Late Cenozoic shortening in the west-central Alborz Mountains, northern Iran, by combined conjugate strike-slip and thin-skinned deformation. Geosphere 2:35–52

Haghnazar, Sh (2009) Petrology and geochemistry of mafic rock in Javaher Dasht area, East of Gillan Province, North of Iran. PhD thesis in Shahid Beheshti University, Tehran, Iran

Havette A, Clocchiatti R, Nativel P, Montaggioni L (1982) Une pargenése inhabituelle àfassaıte, melilite et rhönite dans un basalte alcalin contaminé au contact d'un récif corallien (Saint- Leu, Ile de la Réunion). B Mineral 105:364–375

Huckenholz H, Kunzmann T, Spicker C (1988) Stability of titanian magnesio-hastingsite and its breakdown to rhönite bearing assemblages. Terra Cognita 8:66

Jannot S, Schiano P, Boivin P (2005) Melt inclusions in scoria and associated mantle xenoliths of Puy Beaunit volcano, Chaîne des Puys, massif central, France. Contrib Mineral Petr 149:600–612

Johnston AD, Stout JH (1985) Compositional variations of naturally occurring rhönite. Am Mineral 70:1211–1216

Kelsey CH, McKie D (1964) Thc unit-cell of aenigmatite. Mineral Mag 39:86–1001

Kogarko LN, Hellebrand E, Ryabchikov ID (2005) Trace element partitioning between Rhönite and silicate melt in Cape Verde Volcanics. Geokhimiya 1:3–9

Kóthay K, Szabó CS (1999) Silicate melt inclusion study on olivine phenocrysts from the Hegyestű basalt, Balaton Highland, Hungary. Terra Nostra, 99/6, 15th ECROFI XV, Potsdam, June 21–24, 1999. Abstracts, 170–173

Kóthay K, Szabó CS, Sharygin VV, Török K (2001) Silicate melt inclusion study on olivine phenocrysts and clinopyroxene microphenocrysts in the Hegyestű basalt, Bakony-Balaton highland, Hungary. Memórias 7:237–240

Kristan-Tollmann E, Tollmann A, Halnedani A (1979) Beitraige zur Kenntnis der Trias yon Persien. I. Revision der Triasgliederung, Rhfit fazies im raum yon Isfahan und Kossener Fazieseinschlag bet Waliabad SE Abadeh. Mitt Oster Geol Ges 70:186–119

Kuehner SM, Irving AJ (2007) Primary ferric iron-bearing rhönite in plutonic igneous angrite NWA 4590: implications for redox conditions on the angrite parent body. EOS (Transactions of the American Geophysical Union), 88, Fall Meeting Supplement, Abstract P41A–0219

Kunzmann T (1989) Rhönite: Mineralchemie, Paragenese und Stabilität in alkalibasaltischen Vulkaniten (Ein beitrag zur Mineralogenese der Rhönite-Änigmatit-Mischkristallgruppe). Dissertation. Ludwig-Maximillians-Universität, München, Germany

Kyle PR, Price R (1975) Occurrences of rhönite in theMcMurdo volcanic group, Antarctica and Otago volcano, new Zealan. Am Mineral 60: 722–725

Lacroix MA (1909) Note sur la rhönite du Puy de Barneire à Saint-Sandoux. B Soc Fr Mineral Cr 32:325–331

Leoni L, Saitta M (1976) X-ray fluorescence analysis of 29 trace elements in rocks and mineral standards. Rend Soc Ital Mineral Petrol 32: 497–510

Magonthier MC, Velde D (1976) Mineralogy and petrology of some tertiary leucite- rhönite basanites from Central France. Mineral Mag 40:817–826

McDonough WF, Sun SS (1995) Composition of the earth. Chem Geol 120:223–253

Mineral Data Publishing Version 1.2 http://www.handbookf. Mineralogy. org/pdfs/rhönite/ pdf. 2001

Morata D, Higueras P (1996) Analcimas en lavas alcalinas delSinclinal de Almadén, Origen primario o secundario? Implicacionespetrogenéticas. Boletín de la Sociedad Española de Mineralogía 19:27–37

Morimoto N, Fabries J, Fergusson AK, Guizbourg ID, Ross M, Seifert FA, Zussman J, Aoki K, Gottardi G (1988) Nomenclature of pyroxenes. Am Mineral 173:1123–1133

Nabavi MH, Seyed Emami K (1977) Sinrmurian ammonites from the Shemshak formation of the North Iran (Semnan area. Alborz). N Jb Geol Palaont Abhand 153:70–85

Nakamura N (1974) Determination of REE, Ba, Mg, Na and K in carbonaceous and ordinary chondrites. Geochimica et Cosmichimica Acta 38:757–775

Nazari H, Shahidi A (2011) Tectonic of Iran « Alborz ». Gological Survey and Mineral Exploration of Iran, Research institute for Earth Science

Nazari H, Omrani J, Shahidi, AR (2004) Geological map of Anzali, Scale 1:100000, Geological Survey of Iran

Nazarov, MA, Patchen A, Lawrence, AT (2000) Rhönite bearing Ca, Al-rich inclusions of the Efremovka (CV3) chondrite. In: Lunar and Planetary Science XXXI, Abstract 1242, Lunar and Planetary Institute, Houston (CD-ROM)

Nedli Z, Toth TM (2003) Petrography and mineral chemistry of Rhönite in ocelli of alkali basalt from villany mts, SW Hungary. Journal of the Department of Mineralogy, Geochemistry and Petrology, University of Szeged (Hungary) 44:1123–1133

Nimis P (1995) A clinopyroxene geobarometer for basaltic systemsbased on crystal-structure modeling. Contrib Mineral Petrol 121:115–125

Nimis P, Taylor WR (2000) Single clinopyroxene thermobarometry for garnet peridotites. Part I. Calibration and testing of a Cr-in-Cpx barometer and an enstatite-in-Cpx thermometer. Contrib Mineral Petrol 139:541–554

Nimis P, Ulmer P (1998) Clinopyroxene geobarometry of magmatic rocks. An expanded structural geobarometer for anhydrous and hydrous, basic and ultrabasic systems. Contrib Mineral Petrol 133: 314–327

Olsson HB (1983) Rhönite from Skane (Scania), southern Sweden. Geol Foren Stock For 105:299–286

Onuma K (1983) Effect of oxygen fugacity on Fassaitic pyroxene. J Fac Sci Hokkaido Univ 20:185–194

Peters TJ, Menzies M, Thitlwall M, Kyle PK (2008) Zuni-Bandera volcanism, Rio Grande, USA–melt formation in garnet- and spine-facies mantle straddling the asthenosphere–lithosphere boundary. Lithos 102:295–315

Pouchou JL, Pichoir F (1984) Un nouveau modèle de calcul pour la microanalyse quantitative par spectrométrie de rayons X. La Recherche Aérospatiale 3:167–192

Sabzehei M (1993) Calendrier de la migration permo-triasique et morcellement mésozoique des éléments continentauz de l Iran, These, Univ. Pierre et Marie Curie, Paris, France

Saeedi A (1993) Geological map of Baladeh (1/100000). Geological Survey of Iran, Tehran

Sengör AMC (1990) A new model for the late Paleozoic- Mesozoic tectonic evolution of Iran and implications for Oman. In: Searle MP, Ries AC (eds) The geology and tectonics of the Oman region. Geological Society [London], London, pp. 797–831

Sengör AMC, Natalin BA (1996) Paleotectonics of Asia: fragments of a synthesis. In: Yin A, Harrison M (eds) The tectonic evolution of Asia. Cambridge University Press, Cambridge, pp. 486–640

Sengör AMC, Altiner D, Cin A, Ustaomer T, Hsu KJ (1988) Origin and assembly of the Tethyside orogenic collage at the expense of Gondwana land. In: Audley-Charles MG, Hallman A (eds) Gondwana and Tethys, vol 37. Geological Society, London Special Publication, pp. 119–181

Seyed emami K (2003) Triassic in Iran. Facies 48:91–196

Shahidi A (2005) Evolution tectonique et géodynamique des chaines de l Alborz et du Kopet-Dagh (Iran) depuise le Mésozoique. Journées des Doctorants, 3 et 4 mai, Ecole des Mines de Paris

Shahidi A (2008) Evolution tectonique du Nord de L Iran (Alborz et Kopet-Dagh) depuis le Mésozoique. PhD Thése, Université Pierre et Marie Curie, Paris

Sharygin, VV (2002) Melt Inclusions in Olivine from Mahtesh Ramon Basanite, Southern Israel. Abstracts of reports at the All Russia seminar, Geochemistry of Igneous Rocks, The Alkaline Magmatism on Earth ttp://alkaline2002. narod.ru/ abstracts/ sharigin .html

Sharygin VV, Kóthay K, Petö M, Török K, Timina TJ, Vapnik Y, Kuzmin DV, Szabó CS (2003) Rhönite in alkali basalts: studies of silicate melt inclusions in olivine phenocrysts. ECROFI XVII, 5–7 June, 2003, Budapest, Acta Min.-Petr., Abstract Series 2, Szeged, 2003, 182–183

Sisson TW, Grove TL (1993) Temperatures and H2O contents of low-MgO high-alumina basalts. Contrib Mineral Petrol 113:167–118

Soellner J (1907) Über Rhönit, ein neues aenigmatitähnliches Mineral und über das Vorkommen desselben in basaltischen Gesteinen. Neues Jb Miner Abh 24:475–547

Soffel HC, Förster HG (1984) Polar wander path of the central-East-Iran microplate including new results. N Jahrb Geol Paläontol Abh 168: 165–172

Stampfli GM (1996) The intra-alpine terrain: a Paleotethyan remnant in the alpine Variscides. Eclogae Geol Helv 89:13–42

Stampfli, G.M., 2000. Tethyan oceans. In: E. Bozkurt, J.A. Winchester and J.D.A. Piper (Eds.), Tectonics and magmatism in Turkey and surrounding area. Geological Society of London, Special Publication 173:163–185

Stampfli GM, Marcoux J, Baud A (1991) Tethyan margins in space and time. Palaeogeogr Palaeocl 87:373–409

Steiger R (1966) Die geologie der west-Firuzkuh area (Zentralelburz/Iran). Mitteilungen aus dem Geologischen Institut der Eidgen6ssischen Technischen Hochschule und der Universitiit Zurich

Stocklin J (1974) Northern Iran: Alborz Mountains. In: Spencer AM (ed) Mesozoic–Cenozoic orogenic belts; data for orogenic studies; alpine-Himalayan orogens, vol 4. Geological Society, London Special Publication, pp. 213–234

Streckeisen AL (1974) Classification and nomenclature of plutonic rocks. Recommendations of the IUGS Subcommission on the Systematics of igneous rocks. Geologische Rundschau. Internationale Zeitschrift für Geologie, Stuttgart, pp. 773–785

Taraz H (1974) Geology of the Surmaq-Dehbid area, Abadeh region, Central Iran. Internal report, Geological Survey of Iran, Tehran 138:1–37

Timina TY, Sharygin VV, Golovin AV (2006) Melt evolution during the crystallization of basanites of the Tergesh pipe, northern Minusinsk depression. Geochem Int 44:752–770

Vahdati Daneshmand F (2004) Geological map of Marzanabad (1/100000). Geological Survey of Iran, Tehran

Völlmer T (1987) Zur Geologie des nordlichen Zentral-elburz zwischen Chalus-und Haraz-Tal. In: Mitteliungen aus dem Geologisch-Palaontologischen, vol 63. Institut der Universitat Hamburg, Iran, pp. 1–125

Walenta VK (1969) Zur kristallographie des Rhönits. Z Kristallogr 130: 214–230

Zanchi A, Berra F, Mattei M, Ghassemi M, Sabouri J (2006) Inversion tectonics in central Alborz, Iran. J Struct Geol 28:2023–2037